Active Throttle Control Model for a Small Unmanned Aircraft Turboelectric Power System

Kylar J. Moody[1]

Oklahoma State University, Stillwater, OK, 74078

Small, electrically-powered, unmanned aircraft are limited in range and endurance due to inherently low energy density of batteries, prompting the development of hybrid gas-electric power systems. Previous studies have evaluated electrical system characteristics and suggest that one of the challenges for developing turboelectric power for small unmanned aircraft is the need for active throttle control of the turboshaft engine. An overall system transfer function must be developed and evaluated thoroughly to determine the best type of control algorithm to follow. Preliminary bench tests with a KingTech K60TP 7.3kW turboshaft engine coupled to an electric generator demonstrated turbine stall, electrical system instability, and sluggish overall system response. Measurements included generator shaft speed, as well as rectified power, voltage and current. Results of the system dynamic behavior form a basis for developing a mathematical model that includes both empirical and theoretical turbine behavior. The model proposed in this study uses a new turbine engine transfer function paired with known generator-rectifier characteristics and is evaluated over a turbine operating range. Results indicate the need to incorporate a battery into the power system to enable a faster, more stable active throttle control response.

I. Nomenclature

c_{pc} = specific heat of cold section
c_{pt} = specific heat of hot section
h_{PR} = enthalpy of combustion
i_{DC} = rectified DC current
I = mass moment of inertia for generator
K_F = friction torque coefficient for generator and coupler
K_T = torque coefficient generator
$\dot{m}_c$ = mass flow rate of turbine core
$\dot{m}_f$ = mass flow rate of fuel
P_{elec} = load electrical power
P_{mech} = engine shaft power
T_{T2} = compressor total inlet temperature
T_{T3} = combustor total inlet temperature
T_{T4} = HPT total inlet temperature
$T_{T4.5}$ = PT total inlet temperature
T_{T5} = PT total exit temperature
V_{DC} = rectified DC voltage
γ = ratio of specific heats
η_{elec} = electrical system efficiency
η_{gen} = generator voltage efficiency
η_{mech} = power turbine shaft efficiency
η_{rect} = rectifier efficiency
η_{sc} = shaft coupler mechanical efficiency
π_b = total pressure ratio across combustor
π_c = total pressure ratio across compressor
π_d = total pressure ratio across inlet

[1] Research Assistant, Mechanical & Aerospace Engineering, 201 General Academic Bldg., AIAA Student Member

π_n = total pressure ratio across nozzle
π_{pt} = total pressure ratio across power turbine
π_r = total pressure ratio streamtube
π_{th} = total pressure ratio across high pressure turbine
τ_s = engine output shaft torque
ω_s = generator shaft angular velocity

II. Introduction

Hybrid systems are rapidly developing to meet the needs of the developing Small Unmanned Aerial Systems (SUAS) market. SUAS are defined by the FAA[1] in Part 107 as aircraft which weigh less than 55 pounds (including payload) at takeoff; they must also fly in class G airspace within visible line of sight, and below 400 ft. of ceiling at speeds below 100 miles per hour without a waiver. With both commercial and defense SUAS users imposing rigorous mission requirements such as heavy lift capabilities, long range, increased hover endurance, and short takeoff and recovery, the SUAS market is leaning heavily on hybrid electric systems. Hybrid systems offer significant advantages over conventional electric and gas propulsion systems, combining the high power density of batteries with the high energy density of hydrocarbon fuels. Hydrocarbon fuels are on average around 75 times more energy dense than current Level of Technology (LOT) batteries, making them more desirable for long range or long endurance missions. Batteries, however, have a higher power density with the capability to discharge at rates of over 400 amps; this is desirable for takeoff, hover, Vertical Takeoff and Landing (VTOL), Short Takeoff and Landing (STOL), as well as other mission requirements. The XFold Travel 12 dodecacopter[2] and Oklahoma State University designed Talos are examples of platforms which could benefit from the inclusion of a hybrid power system.

Figure 1. XFold Travel 12 multirotor (left) and the Oklahoma State University designed Talos UAV (right).

There are multiple piston-based hybrid systems that have been developed for both multirotor and fixed-wing applications, however piston-based systems present an array of issues. Though generally more fuel efficient, issues such as cylinder wall cooling, vibration, thermal management, and shaft speed limits the potential of piston-based hybrid systems. Turbine-based hybrid systems are still in development and offer a higher power to weight ratio compared to a piston engine, thus turboelectric systems can have a lower deadweight mass fraction than a comparable piston hybrid system. Turboelectric and other hybrid gas-electric propulsion and power systems are not only being researched in the UAS market, but the increased need for longer range and endurance has driven customers in both the commercial and defense market to explore hybrid systems. NASA has been investigating the use of distributed turboelectric propulsion for passenger aircraft for several years[3], but the scale of these platforms necessitates technologies such as superconducting motors, generators, and cryogenic coolers. SUAS platforms operate on much lower power scales with lower heat transfer rates, allowing for simple convective cooling approaches. In 2011, the Intelligence Advanced Research Projects Agency (IARPA)[4] announced the Great Horned Owl program to develop fuel-to-electricity systems that group air-breathing propulsion systems with power generation systems used to power electric propulsion systems. Rotramel[5] at Air Force Institute of Technology further explored this concept looking at clutch-start parallel configuration on SUAS, in which a combustion engine and electric motor/generator power a common shaft. McKinney[6] of Oklahoma State University discussed issues encountered when employing a piston-based hybrid system, such as overall propulsion system weight and added complexity, which included an additional electrical efficiency term. In general, for small combustion engines, geometric constraints lead to low compression ratios; low compression prior to combustion is the driving factor of poor thermal efficiency. The hybrid-gas system proposed in this study can retain and potentially increase overall system efficiency by distributing power to multiple propulsors. The objective of this study is to characterize the

electromechanical and mechanical system and model the coupled behavior. This overall system transfer function will later be used to develop an active throttle control algorithm to control the turboelectric propulsion system motivating this study.

III. Background

Previous testing of the turboelectric system shown in the schematic of Fig. 2 was performed at Oklahoma State University by Jones and Replogle[7] and resulted in the characterization of the electrical system. The setup consisted of a KingTech K60TP G2 turboprop engine, mechanically coupled to a three-phase generator and three phase full bridge rectifier. In their study, the system was driven electrically by an Electronic Speed Controller (ESC) and compatible motor to easily quantify the transmission losses and electrical efficiency associated with power conversion.

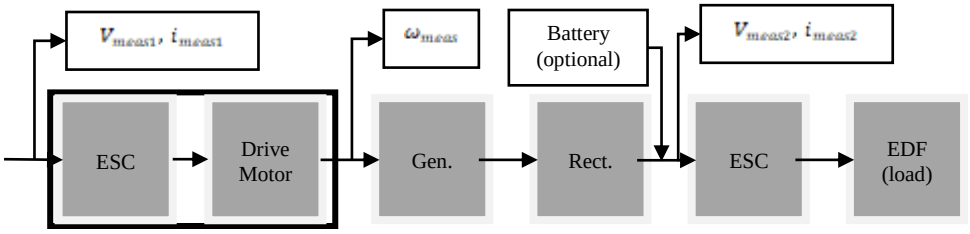

Figure 2. Schematic of the test setup performed by Jones and Replogle.

Jones and Replogle's study reported the effects of varying load current draw on the generator voltage and angular speed for a series configuration turboelectric system. The results of their study confirmed the linear relationship of voltage and angular speed for a particular load. The results for electrical efficiency also agreed with the results obtained by Hageman and Wisniewski[8] for the system electrical efficiency of between 0.6 and 0.7 for a series hybrid configuration. The key results of their study are shown in Fig. 3.

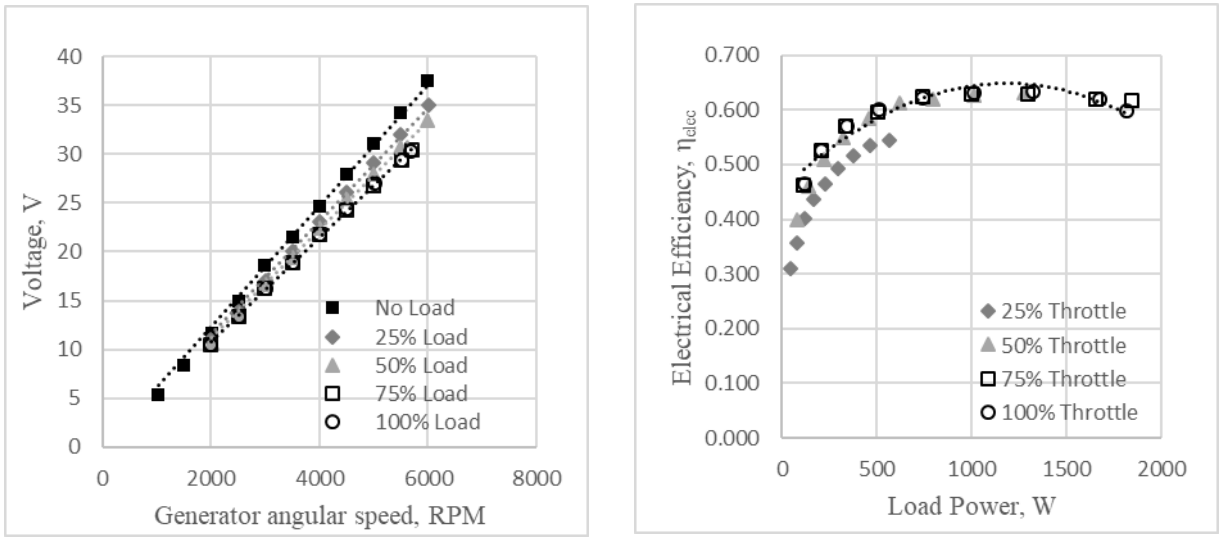

Figure 3. Results of previous turboelectric testing performed.

The same test matrix was attempted unsuccessfully with a turboprop incorporated into the system as shown in Fig. 4. The KingTech K60TP turboprop engine replaced the electric drive motor in the final system. In the experimental setup, two Electric Ducted Fans (EDFs) were used to simulate a load. This effectively acted as dynamometer in a very similar way to an eddy current brake. Loading in this aspect is referred to as an increased throttle input to the EDF which allows more current flow to the load.

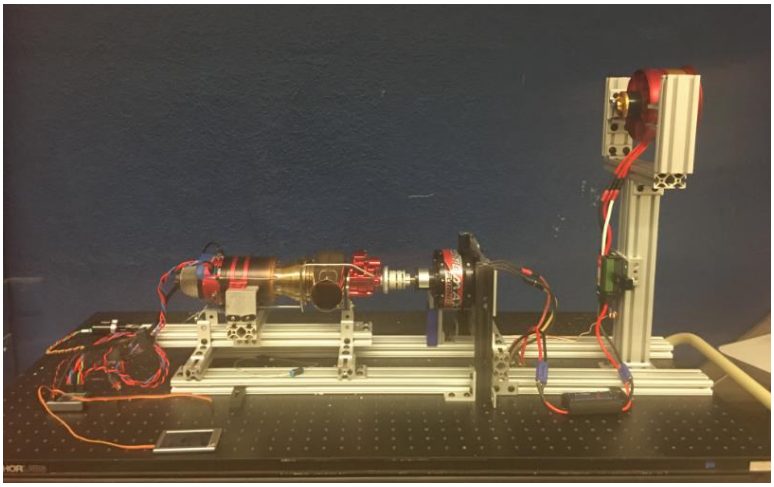

Figure 4. Experimental setup with turboprop engine, generator, rectifier, and load.

One result of the unsuccessful testing was the discovery of unfavorable control characteristics. An electrical system instability caused power turbine stall, which resulted in premature termination of the test on multiple occasions. The electrical load has a much faster response time than the mechanical system driving the power generation system. Ohm's Law states that the decreased resistance allows more current to flow to the load; this is reflected in the generator in the form of an ElectroMotive Force, or back EMF. Back EMF is defined as the voltage generated when the armature rotates inside a magnetic field; this agrees with Lenz's Law, which states that current in a circuit generated from motion in a magnetic field is directed opposite as the change in flux, and exerts a force in the opposing direction[9,10]. This rapid increase in torque occurs before the mechanical system has time to respond, even if the throttle of both systems were brought up simultaneously. Because the response time of the electrical system is about one-fifth the response time of the mechanical system, the turbine power is effectively remaining constant while the torque required increases. This caused a decrease in shaft speed, which increased the power turbine stage loading and initiated a turbine stall. This instability led to the conclusion that an active throttle control model is necessary to accurately and effectively characterize and control the system with a turbine engine incorporated.

A. Turbine Theory

Mattingly and Boyer[11] give the equations of motion for a dual spool turboshaft engine. Several assumptions must be made when analyzing the simplified turbine, which include: isentropic compression and expansion, the turbine casing is "well insulated", exhaust velocity is assumed sufficiently low enough to be neglected, and the inflow is incompressible. Also, because the compressor, high pressure turbine (HPT), and power turbine (PT) are single staged, the polytropic efficiency can be assumed approximately one. Applying these assumptions and performing power balances across the HPT and compressor, the PT and output shaft, and the combustor, Eqs. 1-3 are developed, respectively.

$$\dot{m}_c c_{p_c}(T_{T3} - T_{T2}) = (\dot{m}_c + \dot{m}_f) c_{p_t}(T_{T4} - T_{T4.5})\eta_{mech} \tag{1}$$

$$\eta_{mech}(\dot{m}_c + \dot{m}_f) c_{p_t}(T_{T4.5} - T_{T5}) = \tau_s \omega_s \tag{2}$$

$$(\dot{m}_c + \dot{m}_f) c_{p_t} T_{T4} - \dot{m}_c c_{p_c} T_{T3} = \dot{m}_f h_{PR} \tag{3}$$

Operability starts to become an issue when there is too much backpressure. This means the power turbine is trying to expand the flow beyond ambient pressure. The isentropic flow relation shown in Eq. 4 gives the lower limit of total to static pressure, which occurs at the static case where the Mach number at station nine is equal to zero.

$$\frac{P_9}{P_{T9}} = \left(1 + \frac{\gamma_t - 1}{\gamma_t} M_9^2\right)^{\frac{-\gamma_t}{\gamma_t - 1}} \tag{4}$$

One other relationship for total pressure to static pressure can be shown in Eq. 5 by stepping through each component on the turbine engine core. The freestream pressure ratio, π_r, term is assumed to be 1 for hover and incompressible flow. The inlet pressure ratio, π_d, and nozzle pressure ratio, π_n, term will be assumed approximately 1 and constant for the duration of the mission. The compressor pressure ratio, π_c, and high pressure turbine pressure ratio, π_{th}, come from a power balance; the burner pressure ratio π_b, is less than 1 but is unknown at this time. The total pressures are related by the total temperatures obtained through the power balance by Eq. 6.

$$\frac{P_{T9}}{P_9} = \pi_r \pi_d \pi_c \pi_b \pi_{th} \pi_{pt} \pi_n \frac{P_0}{P_9} > 1 \tag{5}$$

$$\frac{T_{T(i+1)}}{T_{T(i)}} = \left[\frac{P_{T(i+1)}}{P_{T(i)}}\right]^{\frac{\gamma}{\gamma-1}} \tag{6}$$

The total temperature at station two is governed by the ambient temperature as there is no total pressure difference. Total temperature at station three is a function of π_c as shown by Eq. 6. The Clausius inequality denotes entropy must increase across the combustor, thus isentropic relations cannot be used, and total temperature is purely a function of fuel flow rate. Fuel flow rate is a reaction to throttle input. The total temperature at station five is assumed to be equal to the temperature at station nine because the total pressure is conserved, however this value is not measured by default. The temperature between the HPT and PT stage will be known because it is measured by the turbine ECU. The simplified Brayton cycle can be illustrated with the Temperature-Entropy (T-s) diagram in Fig. 5. An increase in the fuel flow rate will cause an increase in π_c and a proportional decrease in π_{th} to satisfy the power balance. Total temperatures at stations (3-9) will also increase, however pressure lines diverge as more heat and entropy is added, thus more PT work can be extracted at higher throttle settings even though the exit fluid temperature is much higher. Comparison of the distance between $T_{T4.5}$ and T_{T9} between the new and old cases on the T-s diagram yields this result.

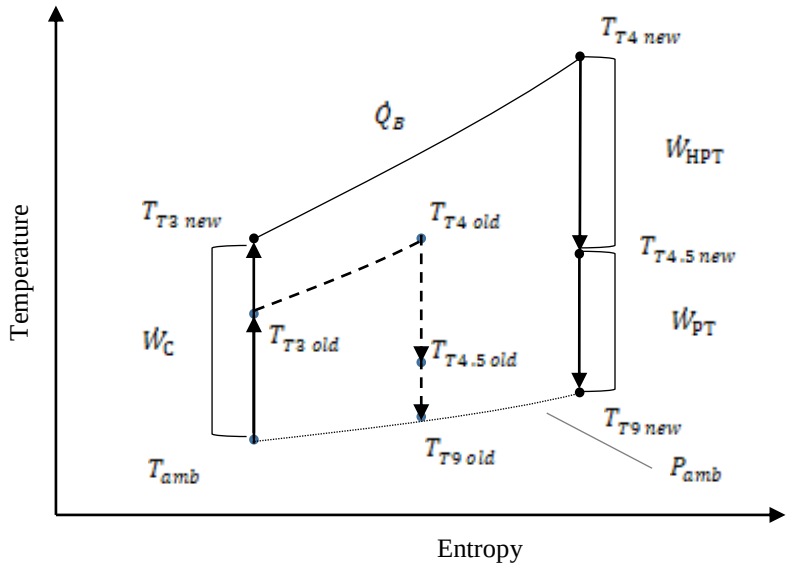

Figure 5. Ideal Brayton cycle T-s diagram showing effect of increasing throttle.

IV. Development of Model

A. Derivation of Generator and Rectifier Model

The electrical system consists of a drive motor, a generator, and a three-phase full bridge rectifier, as shown in the block diagram below. The drive motor can either be an electric motor or gas turbine engine depending on the test matrix, which components are being isolated, and the load power requirements. When testing to validate a system model, an electric motor will be used to drive the system, allowing for isolation of generator and rectifier. The properties of each component can also be shown in the block diagram below. The electro-mechanical system

dynamics analysis was completed using a power balance across components. Some reasonable initial assumptions had to be made about the electrical system as a whole in order to get started; one of these assumptions was to neglect heat loss from the generator. The generator is an out-runner style, thus, does not require additional cooling. If this proves to be a significant source of error in the model, additional considerations will be made. It is also reasonable to assume that all rotational components are rigid, and do not deform under load; this is especially important when developing a model for the rotational components as there is not a spring force acting on the generator casing.

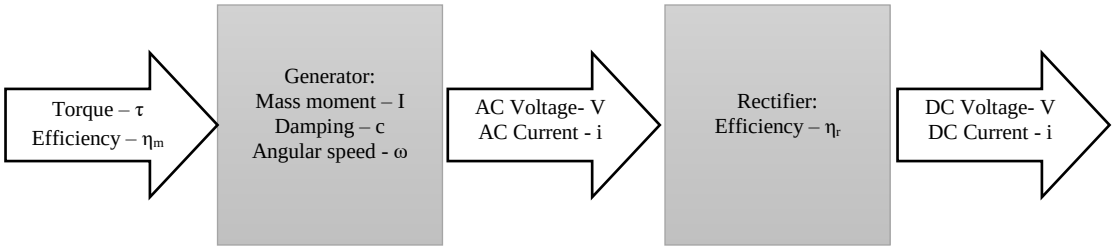

Figure 6. Block diagram of turboelectric power generation system.

A power balance was performed across the generator, using the equations given below; the difference in input and output power is related to the rate of change of energy of the system: kinetic, potential, thermal, and work namely. This can be acquired by differentiating Eq. 7. By modeling the generator as a rigid body, potential energy (PE) in the form of strain energy can be neglected, as well as the Q_{motor} term. By reducing the equations and substituting in appropriate power and energy expressions, Eq. 8 is developed, where the power in is a mechanical power, power out is an electrical power, kinetic energy is a rotational term, and the summation of all work terms is the integral for friction and damping. The final unsteady model across the generator is obtained by differentiating Eq. 8 with the chain rule, as shown in Eq. 9. Substitution was used to evaluate the work integral term.

$$P_{in} - P_{out} = \frac{d}{dt}[KE + PE + W_s + Q_{motor}] \tag{7}$$

$$\eta_{sc}\eta_{gen}\tau_s\omega_s - V_{AC}i_{AC} = \frac{d}{dt}\left[\frac{1}{2}I\omega_s^2 + \int c\,\omega_s\,d\theta\right] \tag{8}$$

$$\eta_{sc}\eta_{gen}\tau_s\omega_s - V_{AC}(\omega)i_{AC} = I\dot{\omega}_s\omega_s + c\omega_s^2 \tag{9}$$

Next, a power balance was performed across the rectifier. Having no inertial, work, or energy storage terms, the equation reduces to power and heat terms. For this initial study, heat losses through the rectifier will be neglected. If heat losses prove to be a significant source of error, thermal effects will be considered. Substituting the appropriate expressions for power into Eq. 7, the resulting transient equation across the generator and rectifier can be obtained, as shown in Eq. 11. Equation 5 relates the load power to the turbine shaft power. One final simplification will be done, which is to divide Eq. 11 by an ω and substitute power factor (PF) for DC voltage per angular rate. PF is defined as the rate of change of voltage per angular rate and is supplied by the manufacturer. Lastly, because the system will be tested and operating at or around a set data point for the majority of its mission, the unsteady terms can be neglected yielding the quasi-steady model of the system as given in Eq. 12. This shows an important characteristic of the system: the linear relationship between torque and current. Power factor can be assumed constant, as well as the damping/friction term. The proportion shown in Eq. 13 can be used to test the model, where K_T, the torque constant, is a function of PF and component efficiencies. The intercept term, known as the friction torque coefficient, K_F, is a function of angular rate, damping, and component efficiencies. This term gives the no load torque of the generator.

$$\eta_{sc}\eta_{rect}V_{AC}(\omega)i_{AC} = V_{DC}(\omega)i_{DC} \tag{10}$$

$$\eta_{sc}\eta_{gen}\tau_s\omega_s - \frac{V_{DC}(\omega)i_{DC}}{\eta_{rect}} = I\dot{\omega}_s\omega_s + c\omega_s^2 \tag{11}$$

$$\eta_{sc}\,\eta_{gen}\tau_s = I\dot{\omega}_s + c\omega_s + \frac{PF_{gen}i_{DC}}{\eta_{rect}} \tag{12}$$

Equations 13 and 15 will be used as our steady state model of the system; this is what will be tested to validate our model of the electrical system characteristics before moving forward with integration of the turbine and battery. To test this theory, generator angular speed will be swept from 0-6500 RPM at five evenly distributed load cases between 0 and 100 percent load power. If torque and current are related linearly, it should be indifferent of load and shaft speed. The transient analysis will be completed upon validation of the model.

$$\tau_s = \frac{c\omega_s}{\eta_{gen}\eta_{sc}} + \frac{PF_{gen}i_{DC}}{\eta_{rect}\eta_{gen}\eta_{sc}} \tag{13}$$

$$\eta_{gen}\eta_{rect} = \eta_{elec} \tag{14}$$

$$\tau_s \propto K_T(i_{DC})i_{DC} + K_F(\omega_s)\omega_s \tag{15}$$

B. Combined Turbine/Generator Model

A transfer function to relate turbine fuel flow rate to load current can be developed by combining the power balance performed in Eq. 2 with the combined generator rectifier power balance equation in Eq. 11. The overall system equation relating $T_{T4.5}$ to load current i_{DC} can be seen in Eq. 16. Equations 1 and 5 must be satisfied simultaneously with Eq. 16 for the system transfer function to behave as expected. As stated in the turbine theory section, the total temperature at station 4.5 is a known. The value of T_{T5} can be interpreted thermodynamically as the temperature of the working fluid at ambient pressure with the entropy of $T_{T4.}$

$$\eta_{mech}\eta_{sc}\eta_{gen}(\dot{m}_c + \dot{m}_f)c_{p_t}(T_{T4.5} - T_{T5}) = I\dot{\omega}_s\omega_s + c\omega_s^2 + \frac{PF\omega_s i_{DC}}{\eta_{rect}} \tag{16}$$

C. Pump/ECU Model

The turbine engine model will relate the K60TP turboshaft engine fuel flow rate from the combustor total temperature, to output shaft torque. In order to develop an overall system transfer function, the fuel flow rate must be related to the ECU signal out as this is the input to the system and the output of the control system. Fuel flow rate is a function of pump power; given a set of parameters a physics-based model could be developed, however that is beyond the scope of this experiment, which focuses primarily on mathematical modeling of the electrical system and turbine. Given the large amount of variability in line inertance and resistance, the fuel system model will be experimental. The experimental setup will consist of the KingTech K60TP pump, a nominal capacity of fuel placed at an appropriate head pressure, and an equivalent amount of fuel line and fuel fittings to the integrated system. The ECU output will be monitored and recorded as a function of fuel flow rate, as shown by the block diagram in Fig. 7. The fuel flow rate vs. throttle signal can be shown in the Results section of the paper.

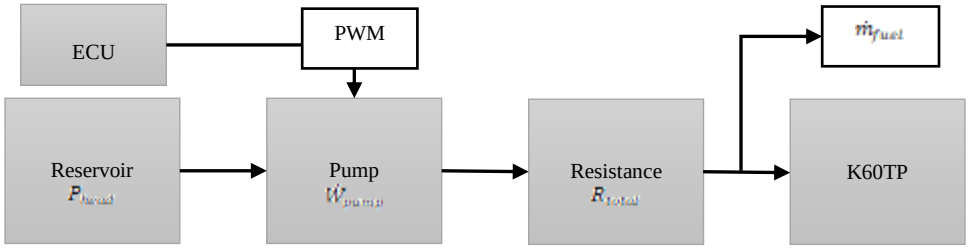

Figure 7. Block diagram of fuel system up to turboprop engine.

V. Results

A. Electrical system testing

1. Torque vs. Current Relationships and Model Validation

Plotted below is Torque vs Current, with torque on the y axis and current on the x-axis. Recall Eq. 9 from the model developed; a linear relationship between torque and current is the anticipated result. Each data point is at a different voltage, angular speed, or load resistance; thus, the relationship holds true that torque is almost purely a function of current. The limiting factor in this model is when voltage and current are considered together, there is a

possibility that the K60TP is not capable of producing enough low-end torque without stalling the PT. This is a function of the PF and the output power rating of the generator.

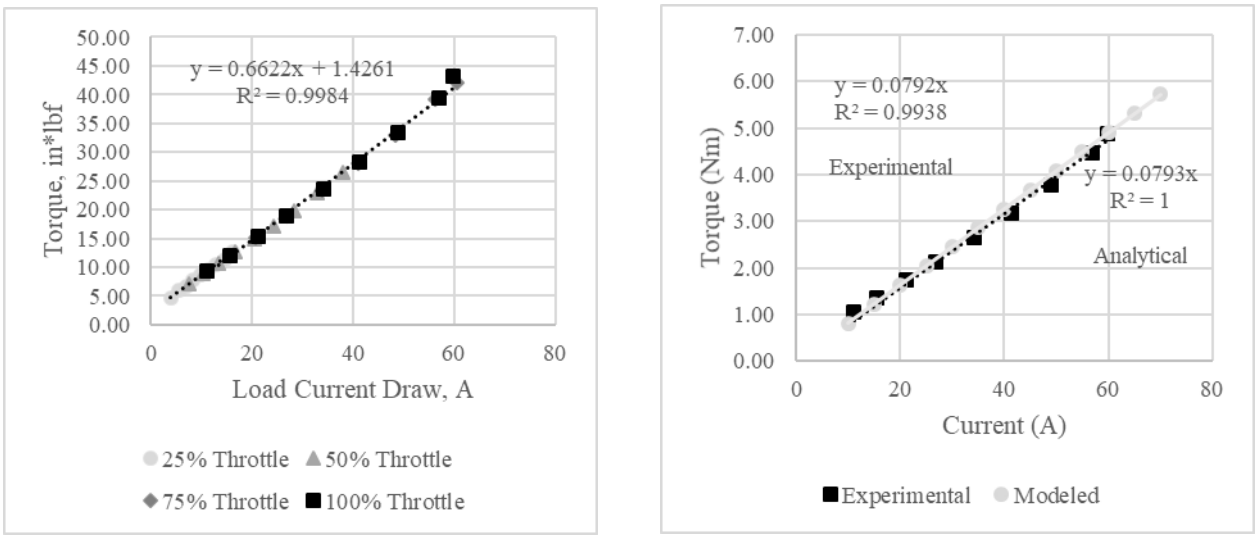

Figure 8. Comparison of torque and current (left) and comparison to model (right).

The modeled values vs the experimental values are also shown in Fig. 8. The table of values assumed for modeling purposes can also be shown in Table 1 below. Jones and Replogle[7] values for electrical efficiency plateaued at 0.63, and the generator PF showed between 1-10% decreases with load. Most multirotor UAS operate with relatively low voltage (22.2V), but with a relatively high current draw (>100A), thus the PF for the maximum loading case will be used for the initial input to the model. The value for PF in the model quotes the manufacturer's specification times the empirical correction factor uncovered by Jones and Replogle.

Table 1. Values used for developing electrical system model.

	Power Factor	Electrical Efficiency	K_T
Modeled Values	(1/167)*0.9	0.63	0.0793

For simplicity in comparison, the modeled values were plotted with a y intercept of zero; for this reason, the experimental curve fit of the data was also fit with a y intercept of zero. This is because the torque is a function of current and angular rate, however the no load torque depends on angular rate and each point is unique in this regard. The torque when subjected to a current load is much greater than the no load torque, for values of current greater than 10 amps, thus the friction term can be neglected for this case.

2. Damping vs. Angular Rate

The value for friction torque coefficient, K_F, across the generator was assumed constant for modeling purposes, therefore must be validated as a reasonable assumption. The values for K_F as a function of angular rate can be shown in Fig. 9. The test was performed by measuring total input power to turn the generator under no load. The no load power of the drive motor was subtracted out, and the remaining power was the rate of work done by friction. Values for K_F were then calculated based on the relation shown in Section IV. Values beyond 3000 RPM show a consistent decrease in magnitude. Though the values for K_F are small, they are not negligible as they scale by ω^2, making overall rate of friction work increase orders of magnitude.

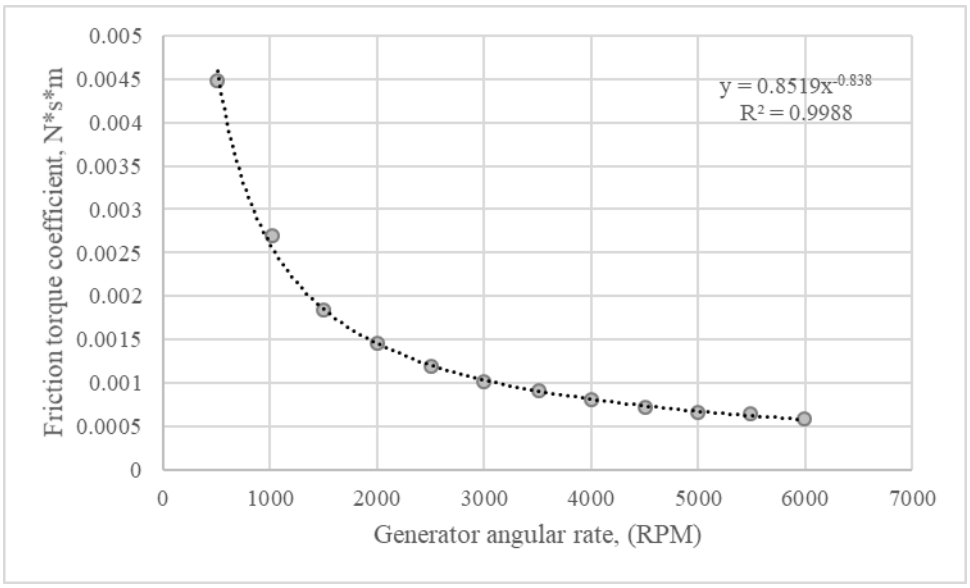

Figure 9. Effect of angular rate on generator damping coefficient.

3. Torque and Angular Rate vs. Voltage and Current

From the model developed in Section IV, torque and current are related linearly. Analyzing the trend observed by Jones and Replogle, voltage and angular rate are linearly related as well. Switching dependent parameters, torque is plotted against angular rate, seen on the left, while voltage is plotted against current, on the right, in Fig. 10 with the related parameters on the same axes. The plot intends to show a side by side comparison of the experimental data which relates the mechanical power, torque and angular rate, to the electrical power, voltage and current. This comparison shows that in the quasi-steady state, the system is behaving as the model expected. The torque vs. angular speed shows some y-intercept, which is predicted in the model as the friction torque coefficient as a function of angular rate. This only appears on the mechanical plot, as the inertial losses occur prior to electrical measurement.

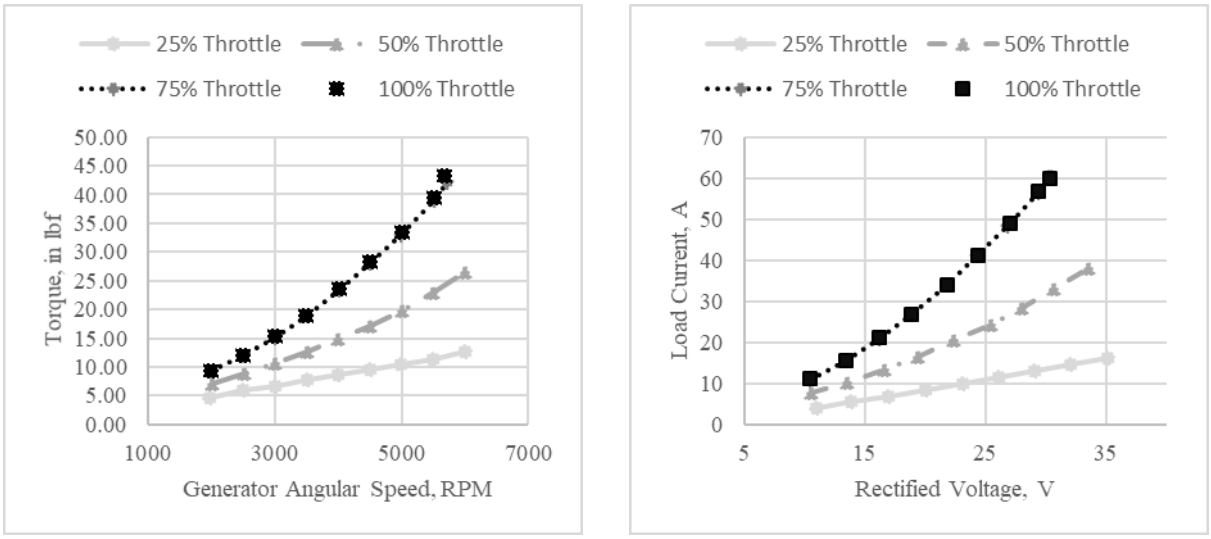

Figure 10. Comparison of torque and angular rate (left) and current and voltage (right) for several load cases.

B. Fuel system response

Pump input signal to pump flow out is a crucial parameter when determining an overall system transfer function. It is important to note the pump requires a Pulse Width Modulation (PWM) input signal, which is similar to a square wave DC voltage signal. The pump sees the duty cycle, or the time between pulses, as a throttle change. The pump was tested at discreet data points and exhibited generally linear behavior between volumetric flow rate and input

signal. This was not necessarily the expected response, as pumps generally exhibit nonlinear performance curves with respect to angular speed. There is an x-intercept, however it is not useful except for predicting the lower bound in the model. Uncertainty was estimated by including the uncertainty of the volume measurement device in the volumetric flow calculation. A beaker with an uncertainty of (±5 mL) volume with resolution of 5 mL was used for flow rates over 1 cc/s, and a graduated cylinder with uncertainty of (±1 mL) and a resolution of 0.2 mL was used for flow rates less than 1 cc/s. These results are valid for a single configuration, as outlined by the block diagram in Fig. 7. If the values of resistance or head pressure are changed in the final integrated system, the test must be repeated as any of these changes would affect the coefficients in the differential equation and change the transfer function.

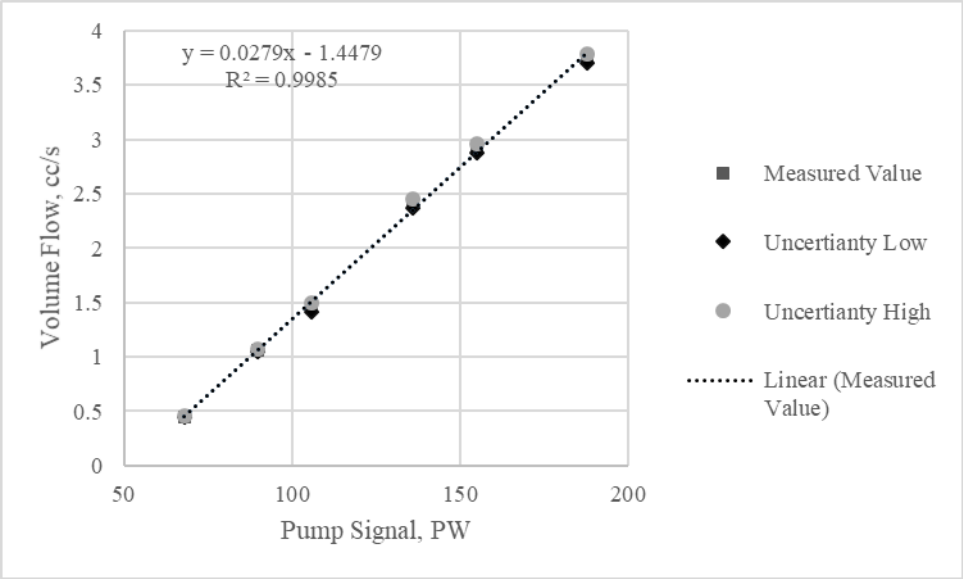

Figure 11. Effect of input signal on volumetric flowrate with uncertainty.

VI. Conclusion and Recommendations

In conclusion, the model developed for the electrical system appears to be a reasonably good start for the development of a full system active throttle control model. The completed system must include a battery for a buffer to prevent power turbine stall, so this will add an extra layer to the model. Modeling showed a pattern in torque and current consistent with literature in this area. One confirmed result was the near instantaneous response time of the electrical system compared to the mechanical system response time. The battery will assist in this sense, picking up some of the slack when an instantaneous input is desired. When the battery is included, the proposed control system would monitor the voltage of the battery and adjust core engine throttle based on whether it is charging or discharging. It would also have to include a feature to update the comparator voltage with the voltage read under the newly adjusted steady operation; this would keep the battery safe as it discharges gradually during the flight regime. At this time, it is believed that proportion control will be sufficient, and the control system will require no direct feedback from the load; the feedback will be obtained indirectly by monitoring the battery voltage. A control system could be implemented without a battery incorporated, however this type of control is not recommended, as it leads to handling issues. The recommended solution is to incorporate a battery and proportion controller, allowing for both closed loop automatic control and more favorable system response.

VII. Acknowledgments

First, I would like to thank our sponsors, Trinity Services Consulting (TSC) Environmental of Enid, Oklahoma as well as the Oklahoma Center for Advancement of Science and Technology (OCAST) for their financial support in the project. I would like to thank Dr. Kurt P. Rouser, my academic and research advisor for providing knowledge, management, and support with the project. I would also like to thank fellow research assistants Nicholas Lucido, Connor McCain, Chase Holland, and Cole Replogle for assisting with testing and fabrication of experimental stand components. Lastly, I would like to thank Dr. Nishantha Ekneligoda for assisting with electrical system theory.

References

[1] https://www.faa.gov/uas/getting_started/part_107/

[2] http://www.xfoldrig.com/xfold-rigs/xfold-travel/

[3] J. Felder, H. Kim, and G. Brown, "Turboelectric Distributed Propulsion Engine Cycle Analysis for Hybrid-Wing-Body Aircraft," AIAA 2009-1132, 47th AIAA Aerospace Sciences Meeting, Orlando, FL, 5-8 January 2009.

[4] Wilson, S. (2011). INTELLIGENCE ADVANCED RESEARCH PROJECTS ACTIVITY (IARPA) - Office of Smart Collection, Great Horned Owl (GHO) Program, Proposers' Day Overview Briefing, IARPA-BAA-11-12, August 15

[5] T. Rotramel, "Optimization of Hybrid-Electric Propulsion Systems for Small Remotely-Piloted Aircraft," MS Thesis, Air Force Institute of Technology, Department of Aeronautics and Astronautics, March 2011.

[6] K. McKinney, "Evaluation of Hybrid-Electric Power System Integration Challenges for Multi-Rotor UAS," MS Thesis, Oklahoma State University, School of Mechanical and Aerospace Engineering, 2018.

[7] L. Jones and C. Replogle, "Characterization of a Turboelectric Power System for Small Unmanned Aircraft," AIAA Student Paper Competition, Region IV, Houston, TX, 29-31 March, 2019 (accepted).

[8] M. Hageman and C. Wisniewski, "Development and Analysis of a Group 1 UAV Series Hybrid Power System with Two Engine Options," AIAA 2016-5011, 52nd AIAA/SAE/ASEE Joint Propulsion Conference, Salt Lake City, UT, 25-27 July 2016. 15D

[9] Hughes, A., *Electric Motors and Drives Fundamentals, Types and Applications,* 3rd ed., Elsevier Science, Burlington, MA. 2006.

[10] Serway, R., and Jewett Jr., J., *Physics for Scientist and Engineers with Modern Physics*, 9th ed., Brooks/Cole, Boston, 2014.

[11] Mattingly, J., and Boyer, K., *Elements of Propulsion: Gas Turbines and Rockets,* 2nd ed., AIAA Education Series, AIAA, New York, 2016.